Bilinear Quadratic Feedback Control of Modular Multilevel Converters

Guacira Costa de Oliveira, Renato Machado Monaro, Gilney Damm, Filipe Perez, Miguel Jimenez Carrizosa

energies

MDPI

Article

Bilinear Quadratic Feedback Control of Modular Multilevel Converters

Guacira Costa de Oliveira [1,2], Renato Machado Monaro [1], Gilney Damm [3,*], Filipe Perez [4] and Miguel Jimenez Carrizosa [5]

[1] Polytechnic School, University of São Paulo (USP), Avenida Professor Luciano Gualberto, 380-Butantã, Sao Paulo 05508-010, SP, Brazil; guacira@alumni.usp.br (G.C.d.O.); monaro@usp.br (R.M.M.)
[2] Laboratoire des Signaux et Systèmes, CNRS-CentraleSupélec-Université Paris Saclay, 91190 Gif-sur-Yvette, France
[3] COSYS-IMSE, Univ Gustave Eiffel, IFSTTAR, F-77447 Marne-la-Vallée, France
[4] SuperGrid Institute, 23 Rue de Cyprian, 69100 Villeurbane, France; filipe.perez@supergrid-institute.com
[5] Centro de Electrónica Industrial, UPM, José Gutiérrez Abascal 2, 28006 Madrid, Spain; miguel.jimenezcarrizosa@upm.es
* Correspondence: gilney.damm@univ-eiffel.fr

Abstract: The present paper introduces the formulation and development of a bilinear quadratic control algorithm for Modular Multilevel Converters (MMCs), with a specific emphasis on achieving internal energy stabilization and balance within the converter. A bilinear average model of the MMC is employed, enabling the separation between the DC voltage and the voltage generated by submodules. The algorithm proposed in this study is formulated using bilinear theory and is founded on quadratic feedback control principles. The stability of the suggested controller is scrutinized using a meticulous mathematical approach based on Lyapunov theory. Subsequently, the theoretical findings are assessed using a comprehensive MMC switching model implemented in Matlab Simscape Electrical. The utilization of a phase-shift PWM technique, accompanied by a sorting algorithm, is considered in the study. Additionally, a comparison between the proposed bilinear controller and a standard PI controller is conducted. The outcomes demonstrate that the proposed controller effectively facilitates the regulation of circulating and AC currents, along with managing the internal energy of MMCs. Consequently, this achievement makes a noteworthy contribution to the field, as it introduces an innovative bilinear control approach capable of stabilizing all the state variables of MMCs converters using a single control law.

Keywords: Modular Multilevel Converter; bilinear control; nonlinear control; Lyapunov theory; Lyapunov stability

Citation: Costa de Oliveira, G.; Machado Monaro, R.; Damm, G.; Perez, P.; Jimenez Carrizosa, M. Bilinear Quadratic Feedback Control of Modular Multilevel Converters. *Energies* **2023**, *16*, 6713. https://doi.org/10.3390/en16186713

Academic Editors: Alon Kuperman and Abu-Siada Ahmed

Received: 4 August 2023
Revised: 13 September 2023
Accepted: 14 September 2023
Published: 19 September 2023

1. Introduction

The current electrical grid comprises a wide variety of energy generation sources (such as hydro, nuclear, wind, or solar plants) connected to consumer centers, regardless of distance [1]. Nowadays, the scenario has become even more complex because renewable generation is intrinsically intermittent and unpredictable. Consequently, managing power flow throughout the entire grid has become a challenge [2]. In this context, High Voltage Direct Current (HVDC) technology offers technical advantages such as increased transmission capacities, reduced transmission losses, independence from the system's frequency, and greater cost-effectiveness compared to AC after a break-even distance [3].

The most recent advancement in the context of converters for HVDC is the Modular Multilevel Converter (MMC) topology. This topology combines the advantages of Voltage Source Converters (VSCs) with increasing voltage levels and lower harmonic production [4–6]. The three-phase MMC topology consists of two arms per phase: upper (u) and lower (l) arms, referring to the leg of the converter that generates the voltage over

and under the neutral point, as depicted in Figure 1. In each arm, there are N submodules (SMs) connected in series, which are switched sequentially to produce $N+1$ voltage levels on the Alternating Current (AC) side of the converter. Each SM is a half-bridge with one capacitor that stores energy, as shown in detail in the figure. Moreover, the SM switching produces a harmonic current that circulates between the arms ($i_{cir,j}$), composed of second-order harmonics as well [7,8]. The MMC has several advantages due to its modular design, including lower switching losses, lower harmonic contents in the output AC voltage, and a smaller station footprint. These advantages give it potential for applications in a wide voltage range [3,9].

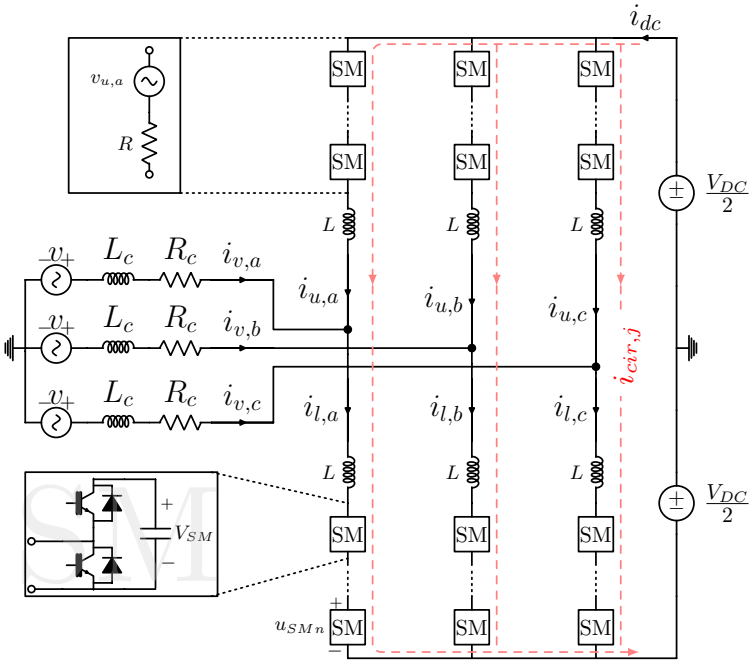

Figure 1. Three-phase MMC.

Significant progress has recently been made in MMC control [10–14]. Approaches based on PI controllers for energy control, voltage oscillation reduction, and DC bus voltage stabilization were proposed by [15,16]. Moreover, in [17], current and energy control, including energy balancing, of a periodic bilinear time-varying state-space MMC model, is achieved by a periodic linear quadratic regulator. In [18], a discrete-time bilinear model of an MMC is developed and controlled using a sum-of-squares decomposition method. Additionally, [19] proposes an analytical filter to eliminate the intrinsic oscillations in the SM capacitor's energy and to improve the dynamic response of the system. Similarly, in [20], a proportional resonant controller aims to regulate the positive and negative sequences of the circulating converter current. Controlling the internal dynamics of an MMC is important to ensure the stability and robustness of the system. Some control schemes that do not consider these internal dynamics may still stabilize the system asymptotically thanks to the linearization in the modulation step. However, these control schemes are less robust because they are prone to poorly damped oscillations on the DC side of the converter. Therefore, it is required to control the MMC's internal dynamics to prevent these issues [9].

In [21], an improved average model is proposed, where a switching function model represents each converter's arm that accurately includes each SM's capacitor dynamics. Furthermore, in [22], a continuous model is used, where a variable-voltage source function describes the arms. A commonality among these models is the increase in system order, leading to heightened complexity in the proposed solutions.

The aforementioned control strategies are mainly based on cascaded control of the arm's energies and the arm's current control loops. As an alternative to these approaches,

the objective of this research is to propose a control strategy capable of individually controlling each of the state variables using a single control law (AC current, circulating current, total energy, and energy distribution among all upper/lower arms). It also aims to provide rigorous proof demonstrating that the proposed control strategy ensures asymptotic stability within the entire region where a Lyapunov function holds (similar to the development in [23] for low-voltage grids). This approach offers the advantage of enabling an explicit computation of the operational region for the proposed controller. The main contributions of this research are summarized as follows:

- a direct control strategy for all state variables of the converter (SM energies and currents);
- a Lyapunov-based stability analysis to demonstrate the suitability of the proposed scheme for asymptotically stabilizing the complex dynamics of the MMC using a single control law.

An average model [18] was used to develop the control, while performance validation was carried out using a detailed MMC switching model implemented in Matlab Simscape Electrical. The switching model includes a low-level controller, which effectively achieves SM voltage balancing. This low-level control has implemented a sorting algorithm based on the standard technique described in [7].

2. Model of a Modular Multilevel Converter

An illustration of an MMC is shown in Figure 1. The N SMs connected in an arm produce a voltage equal to $v_{m,j}$, as shown in detail for upper arm phase a ($v_{u,a}$). It is a three-phase converter and each phase ($j = a, b\ and\ c$) is connected with a leg that consists of upper and lower arms ($m = u\ or\ l$). There are two operational modes for the SMs; mode OFF implies 0 V as output and mode ON entails $V_{SM} = V_{DC}/N$ as output when the system is well-balanced. It is considered that an inductor L is connected in series to each arm of the MMC to limit the short-circuit current and high-frequency harmonics. Additionally, for the average model, the SM switching losses can be represented by an equivalent resistor R. On the AC side, an RL filter is considered per phase (R_c and L_c). Lastly, the voltage at the Direct Current (DC) side is set as $V_{DC}/2$ by the converter on the other side of the transmission line, while on the AC side, $v_{f,j}$ represent the voltage at each phase on the Point of Common Coupling (PCC) with frequency ω.

Based on the MMC circuit shown in Figure 1, an average model can be defined for each phase j by applying Kirchhoff's voltage law as follows:

$$-\frac{V_{DC}}{2} = -v_{u,j} - Ri_{u,j} - L\dot{i}_{u,j} + R_c i_{v,j} + L_c \dot{i}_{v,j} - v_{f,j} \tag{1}$$

$$j = a, b\ and\ c$$

$$\frac{V_{DC}}{2} = v_{l,j} + Ri_{l,j} + L\dot{i}_{l,j} + R_c i_{v,j} + L_c \dot{i}_{v,j} - v_{f,j} \tag{2}$$

The converter currents can be rewritten in terms of $i_{cir,j}$ and $i_{v,j}$ in Equation (3), which are the circulating and AC side currents, respectively [20].

$$i_{cir,j} = \frac{i_{u,j} + i_{l,j}}{2}, \qquad i_{v,j} = -i_{u,j} + i_{l,j} \tag{3}$$

Adding (1) and (2) and replacing Equation (3), one obtains the current dynamic (4) for the phase j from the AC side.

$$\dot{i}_{v,j} = -\frac{R_{eq}}{L_{eq}} i_{v,j} + \frac{v_{u,j} - v_{l,j}}{L_{eq}} + \frac{2v_{f,j}}{Leq} \tag{4}$$

where

$$R_{eq} = R + 2R_c, \qquad L_{eq} = L + 2L_c$$

Considering Park's transformation matrix, the system in *dq0* reference is obtained. Taking into account that, in the equilibrium of balanced systems, the zero component is equal to zero, Equation (4) can be rewritten as system (5), which describes the AC current state variables that should be controlled as follows:

$$\begin{cases} \dot{i}_{v,d} = -\dfrac{R_{eq}}{L_{eq}} i_{v,d} + \omega \cdot i_{v,q} + \dfrac{v_{u,d} - v_{l,d}}{L_{eq}} + \dfrac{2v_{f,d}}{L_{eq}} \\ \dot{i}_{v,q} = -\omega \cdot i_{v,d} - \dfrac{R_{eq}}{L_{eq}} i_{v,q} + \dfrac{v_{u,q} - v_{l,q}}{L_{eq}} + \dfrac{2v_{f,q}}{L_{eq}} \end{cases} \tag{5}$$

By subtracting (2) from (1) and replacing Equation (3), the circulating current dynamic is obtained:

$$\dot{i}_{cir,j} = -\frac{R}{L} i_{cir,j} - \frac{v_{u,j} + v_{l,j}}{2L} + \frac{V_{DC}}{2L} \tag{6}$$

In the *dq*0 frame, (6) can be rewritten as system (7), where $v_{u,0} + v_{l,0} = v_{d0}$ means the DC component in the converter legs. Then, system (7) describes the circulating current dynamics in the *dq0* reference that should be controlled.

$$\begin{cases} \dot{i}_{cir,d} = -\dfrac{R}{L} i_{cir,d} + \omega \cdot i_{cir,q} - \dfrac{v_{u,d} + v_{l,d}}{2L} \\ \dot{i}_{cir,q} = -\omega \cdot i_{cir,d} - \dfrac{R}{L} i_{cir,q} - \dfrac{v_{u,q} + v_{l,q}}{2L} \\ \dot{i}_{cir,0} = -\dfrac{R}{L} i_{cir,0} - \dfrac{v_{d0}}{2L} + \dfrac{V_{DC}}{2L} \end{cases} \tag{7}$$

The operation of an MMC implies voltage changes in the SM's capacitor. In this way, SMs will be used to synthesize the output AC voltage and, as a consequence, to drive the output currents. Based on this, it is possible to directly state that the voltage on SMs' capacitor means a certain amount of stored energy per SM. In this paper, the total amount of energy stored in the entire MMC is considered as a state, as well as the difference between the energy stored on all upper and lower arms. In this approach, proposed by [18], using the MMC's average model, the total stored energy (W_h) is achieved by the converter power balance, which represents the derivative of the converter's energy.

$$\begin{aligned} \dot{W}_h = &-\frac{3}{4} v_{u,d} i_{v,d} + \frac{3}{2} v_{u,d} i_{cir,d} - \frac{3}{4} v_{u,q} i_{v,q} \\ &+ \frac{3}{2} v_{u,q} i_{cir,q} + \frac{3}{4} v_{l,d} i_{v,d} + \frac{3}{2} v_{l,d} i_{cir,d} \\ &+ \frac{3}{4} v_{l,q} i_{v,q} + \frac{3}{2} v_{l,q} i_{cir,q} + 3 i_{cir,0} v_{d,0} \end{aligned} \tag{8}$$

Similarly, the derivative of the energy balance (W_v) is defined as the difference between the stored energy on upper and lower SMs, as shown below:

$$\begin{aligned} \dot{W}_v = &-\frac{3}{4} v_{u,d} i_{v,d} + \frac{3}{2} v_{u,d} i_{cir,d} - \frac{3}{4} v_{u,q} i_{v,q} \\ &+ \frac{3}{2} v_{u,q} i_{cir,q} - \frac{3}{4} v_{l,d} i_{v,d} - \frac{3}{2} v_{l,d} i_{cir,d} \\ &- \frac{3}{4} v_{l,q} i_{v,q} - \frac{3}{2} v_{l,q} i_{cir,q} \end{aligned} \tag{9}$$

Finally, considering the state vector as $x = [i_{v,d}\ i_{v,q}\ i_{cir,d}\ i_{cir,q}\ i_{cir,0}\ W_h\ W_v]^T$ and the controller input as $u = [v_{u,d}\ v_{u,q}\ v_{l,d}\ v_{l,q}\ v_{d0}\ ]^T$, the three-phase MMC can be represented as the following bilinear form:

$$\dot{x} = Ax + \sum_{k=1}^{\rho} B_k u_k x + b_k u_k + z \tag{10}$$

where, considering $\rho = 5$ to represent a three-phase MMC,

$$A = \begin{bmatrix} -\frac{R_{eq}}{L_{eq}} & \omega & 0 & 0 & 0 & 0 & 0 \\ -\omega & -\frac{R_{eq}}{L_{eq}} & 0 & 0 & 0 & 0 & 0 \\ 0 & 0 & -\frac{R}{L} & \omega & 0 & 0 & 0 \\ 0 & 0 & -\omega & -\frac{R}{L} & 0 & 0 & 0 \\ 0 & 0 & 0 & 0 & -\frac{R}{L} & 0 & 0 \\ 0 & 0 & 0 & 0 & 0 & 0 & 0 \\ 0 & 0 & 0 & 0 & 0 & 0 & 0 \end{bmatrix}$$

$$B_1 = \begin{bmatrix} 0 & 0 & 0 & 0 & \cdots & 0 \\ \vdots & \vdots & \vdots & \vdots & \ddots & \vdots \\ 0 & 0 & 0 & 0 & \cdots & 0 \\ -\frac{3}{4} & 0 & \frac{3}{2} & 0 & \cdots & 0 \\ -\frac{3}{4} & 0 & \frac{3}{2} & 0 & \cdots & 0 \end{bmatrix}$$

$$B_2 = \begin{bmatrix} 0 & 0 & 0 & 0 & 0 & \cdots & 0 \\ \vdots & \vdots & \vdots & \vdots & \vdots & \ddots & \vdots \\ 0 & 0 & 0 & 0 & 0 & 0 & 0 \\ 0 & -\frac{3}{4} & 0 & \frac{3}{2} & 0 & 0 & 0 \\ 0 & -\frac{3}{4} & 0 & \frac{3}{2} & 0 & 0 & 0 \end{bmatrix}$$

$$B_3 = \begin{bmatrix} 0 & 0 & 0 & 0 & \cdots & 0 \\ \vdots & \vdots & \vdots & \vdots & \ddots & \vdots \\ 0 & 0 & 0 & 0 & \cdots & 0 \\ \frac{3}{4} & 0 & \frac{3}{2} & 0 & \cdots & 0 \\ -\frac{3}{4} & 0 & -\frac{3}{2} & 0 & \cdots & 0 \end{bmatrix}$$

$$B_4 = \begin{bmatrix} 0 & 0 & 0 & 0 & 0 & \cdots & 0 \\ \vdots & \vdots & \vdots & \vdots & \vdots & \ddots & \vdots \\ 0 & 0 & 0 & 0 & 0 & 0 & 0 \\ 0 & \frac{3}{4} & 0 & \frac{3}{2} & 0 & 0 & 0 \\ 0 & -\frac{3}{4} & 0 & -\frac{3}{2} & 0 & 0 & 0 \end{bmatrix}$$

$$B_5 = \begin{bmatrix} 0 & \cdots & 0 & 0 & 0 & 0 \\ \vdots & \ddots & \vdots & \vdots & 0 & 0 \\ 0 & \cdots & 0 & 0 & 0 & 0 \\ 0 & \cdots & 0 & 3 & 0 & 0 \\ 0 & \cdots & 0 & 0 & 0 & 0 \end{bmatrix}$$

$$b_1 = \begin{bmatrix} \frac{1}{L_{eq}} & 0 & -\frac{1}{2L} & 0 & 0 & 0 & 0 \end{bmatrix}^T$$

$$b_2 = \begin{bmatrix} 0 & \frac{1}{L_{eq}} & 0 & -\frac{1}{2L} & 0 & 0 & 0 \end{bmatrix}^T$$

$$b_3 = \begin{bmatrix} -\frac{1}{L_{eq}} & 0 & -\frac{1}{2L} & 0 & 0 & 0 & 0 \end{bmatrix}^T$$

$$b_4 = \begin{bmatrix} 0 & -\frac{1}{L_{eq}} & 0 & -\frac{1}{2L} & 0 & 0 & 0 \end{bmatrix}^T$$

$$b_5 = \begin{bmatrix} 0 & 0 & 0 & 0 & -\frac{1}{2L} & 0 & 0 \end{bmatrix}^T$$

$$z = \begin{bmatrix} \frac{2v_{f,d}}{L_{eq}} & \frac{2v_{f,q}}{L_{eq}} & 0 & 0 & \frac{V_{DC}}{2L} & 0 & 0 \end{bmatrix}^T$$

3. Bilinear Control Theory

MMCs, as the majority of power electronic converters, can be represented by a bilinear model [24], because their states multiply control inputs as in (10). In the following, we consider a bilinear system with state variables $x \in \mathbb{R}^n$ and input $u \in \mathbb{R}^\rho$.

3.1. Bilinear System Stability—A General Case

There are several ways to study the stability of bilinear systems [25]; however, a direct way to carry out this task is to apply standard Lyapunov theory (see [26,27]).

In this context, the goal is to find a positive definite Lyapunov function candidate V, whose time derivative will be negative definite. In this way, the candidate $V_g : \mathbb{R}^n \to \mathbb{R} > 0$ could be defined as a quadratic function as

$$V_g(x) = x^T P x \tag{11}$$

with a symmetric positive definite matrix $P \in \mathbb{R}^{n \times n}$, and we can compute the derivative of the Lyapunov function:

$$\begin{aligned} \dot{V}_g(x) =& (Ax + \sum_{k=1}^{\rho} B_k u_k x + b_k u_k)^T P x \\ &+ x^T P (Ax + \sum_{k=1}^{\rho} B_k u_k x + b_k u_k) \\ =& x^T [A^T P + PA] x + 2 x^T P \sum_{k=1}^{\rho} u_k (B_k x + b_k) \end{aligned} \tag{12}$$

where

$$(B_k u_k x + b_k u_k)^T P x = x^T P (B_k u_k x + b_k u_k)$$

Under the control law $u_k = -\alpha_s [B_k x + b_k]^T P x$, with a positive constant α_s and the further assumptions that for $k = 1, ..., \rho$, it is true that $(B_k x + b_k)^T P x \neq 0 \ \ \forall x \neq 0$ and that $x^T [A^T P + PA] x \leq 0$ (see [28]), Equation (12) will enter a closed loop:

$$\begin{aligned} \dot{V}_g(x) \leq& -\phi ||x||^2 - 2\alpha_s \sum_{k=1}^{\rho} (x^T P (B_k x + b_k))^2 \\ \dot{V}_g(x) <& 0 \end{aligned} \tag{13}$$

where the constant ϕ is greater than or equal to zero.

Considering $\alpha_s > 0$, Lyapunov's theory assures that the full system is asymptotically stable.

3.2. Bilinear System Stability—Studied Case

Following [29], with the purpose of maintaining the state variable x on a desired operation point $\bar{x}$, we perform a change of variables $x \stackrel{\triangle}{=} \tilde{x} + \bar{x}$, and $u \stackrel{\triangle}{=} \tilde{u} + \bar{u}$.

Applying the change of variables in Equation (10), one obtains (14):

$$\dot{\tilde{x}} + \dot{\bar{x}} = A(\tilde{x} + \bar{x}) + \sum_{k=1}^{\rho} \{(\tilde{u}_k + \bar{u}_k)(B_k(\tilde{x} + \bar{x}) + b_k)\} + z \tag{14}$$

which can be rewritten into two parts, where the input reference values ($\bar{u}_k$) on the equilibrium can be defined as

$$\dot{\bar{x}} = A\bar{x} + \sum_{k=1}^{\rho} \bar{u}_k(B_k\bar{x} + b_k) + z = 0 \tag{15}$$

and then

$$\dot{\tilde{x}} = A\tilde{x} + \sum_{k=1}^{\rho} \bar{u}_k B_k\tilde{x} + \sum_{k=1}^{\rho} (B_k\tilde{x} + B_k\bar{x} + b_k)\tilde{u}_k \tag{16}$$

The evolution of the error states is analyzed by the Lyapunov function and its derivative:

$$V(\tilde{x}) = \tilde{x}^T P\tilde{x} \tag{17}$$

$$\begin{aligned} \dot{V}(\tilde{x}) = & \underbrace{\tilde{x}^T(\tilde{A}^T P + P\tilde{A})\tilde{x}}_{1^{st}\ Term} + \\ & \underbrace{+ 2[\sum_{k=1}^{m} \tilde{u}_k(B_k\tilde{x} + B_k\bar{x} + b_k)]^T P\tilde{x}}_{2^{nd}\ Term} \end{aligned} \tag{18}$$

where $\tilde{A} = A + \sum_{k=1}^{\rho} \bar{u}_k B_k$

$$\tilde{u}_k = -\alpha_k[B_k\tilde{x} + B_k\bar{x} + b_k]^T P\tilde{x} \tag{19}$$

$$u_k = \tilde{u}_k + \bar{u}_k \tag{20}$$

Remark 1. *Because of the MMC model characteristics (shape of A matrix), not all state variables are present in the first part of Equation (18). In this way, this part of the Lyapunov function derivative would only be negative semi-definite. As a consequence, its 2nd part will provide the remaining states.*

Acknowledging these facts, the following procedure based on Lemma 1 of [30] is necessary to design the controller and access the stability properties of the closed loop system.

Matrix $\tilde{A} \in \mathbb{R}^{n\times n}$ has two zero eigenvalues, $\lambda_{n-1}(\tilde{A}) = 0$ and $\lambda_n(\tilde{A}) = 0$, such that $\tilde{A}$ admits the Jordan decomposition $\tilde{A} = U\Lambda U^{-1}$, where $U \in \mathbb{C}^{n\times n}$ is non-singular and Λ is a diagonal Jordan matrix of $\tilde{A}$. Considering $\Lambda_R := diag(\Re e(\Lambda_i))$ for all $i \in [1, n-2]$, then since $\Re e(\lambda_i) < 0\ \forall\ i \in [1, n-2]$, there exists a matrix $\Gamma_R \in \mathbb{R}^{n-2\times n-2}$, symmetric and positive definite, such that $\Gamma_R\Lambda_R + \Lambda_R^T\Gamma_R = -\Phi$, where the diagonal matrices $\Phi \in \mathbb{R}^{n-2\times n-2}$ and $\Gamma \in \mathbb{R}^{n\times n}$ are positive definite, and constants $\Gamma_1, \Gamma_2 > 0$ as follows:

$$\Phi := \begin{bmatrix} \Phi_1 & 0 & 0 \\ 0 & \ddots & 0 \\ 0 & 0 & \Phi_{n-2} \end{bmatrix} \tag{21}$$

$$\Gamma := \begin{bmatrix} 1 & 0 & 0 & 0 & 0 \\ 0 & \ddots & 0 & 0 & 0 \\ 0 & 0 & 1 & 0 & 0 \\ 0 & 0 & 0 & \Gamma_1 & 0 \\ 0 & 0 & 0 & 0 & \Gamma_2 \end{bmatrix} \tag{22}$$

We solve the equation $\Gamma\Lambda + \Lambda^*\Gamma = -Q$, where

$$Q := \begin{bmatrix} \Phi_1 & 0 & 0 & 0 & 0 \\ 0 & \ddots & 0 & 0 & 0 \\ 0 & 0 & \Phi_{n-2} & 0 & 0 \\ 0 & 0 & 0 & 0 & 0 \\ 0 & 0 & 0 & 0 & 0 \end{bmatrix} \tag{23}$$

Then, $P = U^{-T}\Gamma U^{-1}$ is Hermitian positive definite, since Γ is symmetric positive definite and U^{-1} has full rank (see [30]). That implies that $V(x)$ is a real positive definite function. Next, the derivative of the Lyapunov function $\dot{V}(\tilde{x})$ is evaluated as

$$\begin{aligned} \dot{V}(\tilde{x}) = &- \sum_{c=1}^{n-2} \Phi_c ||\tilde{x}_c||^2 + \\ &- 2(\sum_{k=1}^{\rho} \alpha_k ((B_k\tilde{x} + B_k\bar{x} + b_k)^T P\tilde{x})^2) \end{aligned} \tag{24}$$

with $\tilde{x}_c$, Φ_c, $c = 1 \ldots n-2$, the $n-2$ error states not associated with a zero eigenvalue and their exponential decay rates, and where we can show that for typical values $\sum_{k=1}^{\rho} \alpha_k ((B_k\tilde{x} + B_k\bar{x} + b_k)^T P\tilde{x})^2 \neq 0 \ \ \forall \tilde{x} \neq 0$, and as a consequence, $\dot{V}(\tilde{x}) < 0$, $\forall \tilde{x} \neq 0$.

Theorem 1. *The MMC converter described by the system of equations (10), under the bilinear control law described in Equation (19), and with desired equilibrium point satisfying Equation (15), and the assumption that for $k = 1, ..., \rho$, it is true that $(B_k\tilde{x} + b_k)^T P\tilde{x} \neq 0 \ \ \forall \ \tilde{x} \neq 0$, will be asymptotically stabilized towards this equilibrium point, inside the whole domain where the assumption is valid.*

Proof. The proof is standard and is obtained by virtue of the positive definite Lyapunov function (17) of the error system, in which closed-loop derivative (24) is negative definite. Then, by Lyapunov theory, the considered equilibrium point is asymptotically stable. □

Remark 2. *It is important to remark that (24) is negative definite for any tuning parameter value $\alpha_k > 0$ (including all α_k equal to one single value). These parameters indeed set the speed of convergence of the terms $\alpha_k((B_k\tilde{x} + B_k\bar{x} + b_k)^T P\tilde{x})^2 \to 0$. The larger those values, the faster the overall system will converge to its equilibrium point, in a trade-off with the control efforts. It is then necessary to proceed with an optimization strategy for this tuning, even though any chosen value will keep the system stable. Such an optimization study will be carried out in future works.*

In order to use the bilinear control defined above, the references for the state variables and the steady-state inputs must be derived from the desired outputs. Consequently, Equation (15) is solved to obtain $\bar{u}$, as shown in (25) for $c \in [1, n-2]$.

$$\bar{u} = \gamma \quad \bar{x}_c + \zeta \tag{25}$$

$$\gamma = \begin{bmatrix} \frac{R_{eq}}{2} & -\omega\frac{L_{eq}}{2} & -R & w & 0 \\ \omega\frac{L+L_c}{2} & \frac{R_{eq}}{2} & -wL & -R & 0 \\ -\frac{R_{eq}}{2} & \omega\frac{L+L_c}{2} & -R & \omega & 0 \\ -\omega\frac{L+L_c}{2} & -\frac{R_{eq}}{2} & -\omega L & -R & 0 \\ 0 & 0 & 0 & 0 & -2R \end{bmatrix}$$

$$\zeta = \begin{bmatrix} -v_{fd} & -v_{fq} & v_{fd} & v_{fq} & v_{DC} \end{bmatrix}^T$$

Following the AC active and reactive power definitions in Equations (26) and (27) below, the desired values for the AC currents are defined in Equations (28) and (29).

$$P_e = \frac{3}{2} v_{f,d} i_{v,d} \tag{26}$$

$$Q_e = -\frac{3}{2} v_{f,d} i_{v,q} \tag{27}$$

$$\bar{x}_1 = \bar{i}_{v,d} = \frac{2\bar{P}_e}{3v_{f,d}} \tag{28}$$

$$\bar{x}_2 = \bar{i}_{v,q} = \frac{2\bar{Q}_e}{3v_{f,d}} \tag{29}$$

Since the components dq of circulating current in an MMC do not produce useful power, and in addition, they increase the converter losses, they should be minimized. For this reason, their references are taken as zero:

$$\bar{x}_3 = \bar{i}_{cir,d} = 0, \quad \bar{x}_4 = \bar{i}_{cir,q} = 0 \tag{30}$$

Reference for zero component of the circulating current comes from the equilibrium point ($\dot{x} = 0$) of Equation (8), replacing (25) and (30) to obtain Equation (31) as follows:

$$\bar{x}_5 = \bar{i}_{cir,0} = \frac{V_{DC} - \sqrt{V_{DC}^2 - 4R(\bar{x}_1\bar{u}_1 + \bar{x}_2\bar{u}_2)}}{4R} \tag{31}$$

One of the roots is unfeasible since it brings the MMC to a very high dissipating mode, so the other root is chosen.

The reference to SM energy is linked with SMs' capacitor voltage, and this can be expressed as in the following equation:

$$V_{DC} - 2Ri_{cir,j} - 2L\dot{i}_{cir,j} = 2NV_{SM} \tag{32}$$

applying Park's transformation in Equation (32), the equilibrium point for capacitors' voltage is

$$V_{SM} = \frac{V_{DC} - 2R\bar{x}_5}{2N} \tag{33}$$

Then, the stored energy per SM, with capacitor C_{SM}, can be shown as

$$W_{SM} = \frac{1}{2} C_{SM} V_{SM}^2 \tag{34}$$

By Equation (34), considering all active SMs, the total energy of the converter is obtained:

$$\bar{x}_6 = \bar{W}_h = 6 \;\; N \;\; W_c = \frac{3C_{SM}}{4N} \;\; (V_{DC} - 2R\bar{x}_5)^2 \tag{35}$$

Because of the symmetric shape of converters, upper and lower arms should have the same stored energy, W_c^{up} and W_c^{low}, respectively, during steady state, so zero is chosen as the reference for the energy balance:

$$3N \;\; W_c^{up} - 3N \;\; W_c^{low} = \bar{x}_7 = \bar{W}_v = 0 \tag{36}$$

The state reference and the stability condition defined above fuel the simulation test section.

4. Validation of the Proposed Control Strategy

The dynamic performance of the proposed bilinear control strategy applied to an MMC switching model (shown in Figure 1) was verified by computer simulations using the *Matlab Simscape Electrical* environment. The system's parameters and the controller gains are presented in Table 1. The feedback gains were chosen by a trade-off between speed of response and control effort. In this way, the controlled variables could have the speed dynamics of classical power systems. As explained in Remark 2, any positive value chosen for the parameters α_k assures the stability of the equilibrium point. An optimization study would be necessary to set optimal values, which will be carried out in future works. In the present case, all parameters were set to the same value, with already good performance (even if not an optimal performance).

Table 1. Parameters of simulated system and bilinear control's gains.

Parameter	Value	Parameter	Value
S_{MMC}	50 MVA	α_1	0.5
V_{AC}	30 kV	α_2	0.5
V_{DC}	180 kV	α_3	0.5
L_c	5 mH	α_4	0.5
L	14 mH	α_5	0.5
R_c	0.03 Ω	Γ_1	1
C_{SM}	3 mF	Γ_2	1
Freq	60 Hz	Φ_c	1
R	0.5 Ω	N	20

The performance of the proposed bilinear control strategy for the MMC was evaluated through step changes in the converter operating point of variables such as active and reactive power (P_e and Q_e), total stored energy (W_h), and on the energy balance from the upper and lower arms (W_v). The tests were carried out in three-step changes: for active and reactive power, for total stored energy, and for the energy balance. For comparison purposes, a PI control based on [16] was implemented. The PI control was tuned according to [31]. The diagram in Figure 2 summarizes the implementation of PI (white blocks) and bilinear (black blocks) controllers, while gray blocks are common for both controllers.

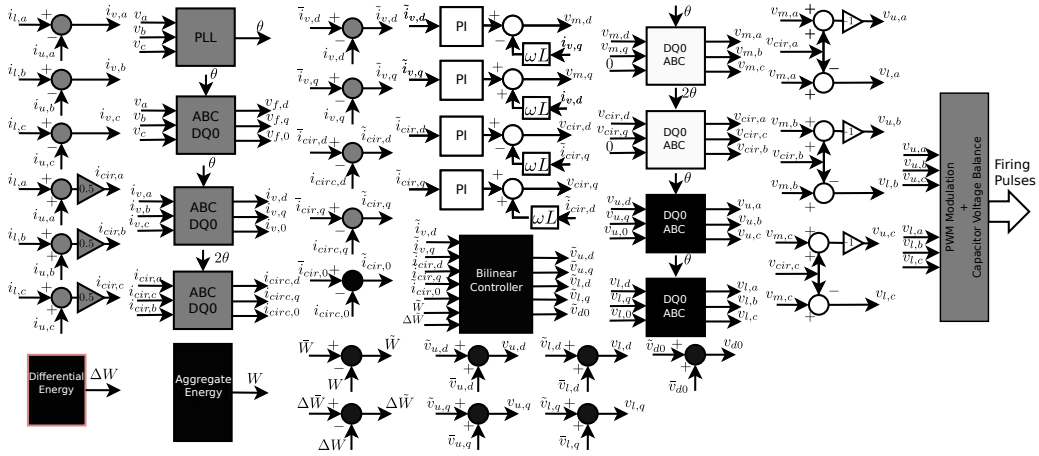

Figure 2. PI and bilinear control diagram.

4.1. Step Changes on Active and Reactive Power References

The performance of the proposed bilinear control strategy for the MMC was first evaluated through step changes on active (P_e) and reactive power (Q_e). Active and reactive power are followed by state variables in Figure 3. The system is initialized, transmitting zero power.

The considered controllers, bilinear, and PI, provide to the states i_{cird} and i_{cir0} different references. So, for those two states, it is written *Ref. Bilinear* to indicate the bilinear controller's reference and *Ref. PI* to identify the PI's references. The remaining states have the same references, indicated as *Ref.*

The second and third graphics represent direct ($i_{v,d}$) and quadrature ($i_{v,q}$) AC currents. These two state variables have a direct relation with the required power, shown in the first graphic.

At $t = [0.05\ 0.15\ 0.25\ 0.45\ 0.55]$ s, the changes in the active power reference occur. In this test, the bilinear and PI controllers were capable of tracking the $i_{v,d}$ reference in less than 4 ms; meanwhile, state $i_{v,q}$ is lightly affected by the changes in P_e. The $i_{v,q}$ follows the change that occurs in reactive power at $t = [0.1\ 0.30\ 0.40]$ s. It can be observed that the controller was capable of bringing $i_{v,q}$ to its reference $\bar{i}_{v,q}$, for all operating points. Furthermore, for both controllers PI and Bilinear, it is possible to see the coupling effect between $i_{v,d}$ and $i_{v,q}$, while the change in one state implies a transient deviation (from the reference) in the other.

Concerning the state variable $i_{cir,d}$, there are distinct references for each controller as a result of each implementation. Under PI, the reference changes from zero for each active power step. However, PI control drives the state variables to their references. In addition to that, Bilinear keeps $i_{cir,d}$ in the $\bar{i}_{cir,d} = 0$. The controllers hold the quadratic component ($i_{cir,q}$) in the desired reference for most of the operating points. When Q_e changes from positive to zero and negative values, the state variables present a slower response under bilinear control (from $t = 0.30$ s).

Directly related to the amount of DC power that is transferred, changes in $i_{cir,0}$ (6th graph) follow the changes in $i_{v,d}$ (directly linked with AC active power). Here again, the control also performs well and the PI time response is around 100 ms and around 10 ms for bilinear. In the seventh graph, the total converter energy is shown, and it swings for each new power operation change. It is clear that this state is slower than the others, as it takes around 200 ms to track the reference again under bilinear control.

The eighth graph shows the energy balance between the upper and lower arms. Controls keep the state variable around the reference, however with a slow speed of convergence. Under bilinear control, energy balancing (W_v) requires more than 150 ms to track its reference, while at the same time, under PI control, state variables require different speeds of convergence according to the operation points.

It is important to highlight that Figure 3 summarizes a number of operating points in a matter of 0.7 s to explore possible control constraints.

Table 2 summarizes the comparison control performance between the proposed bilinear control and the standard PI control. Other important control aspects such as stability, region of attraction, parameter tuning, and robustness are described next, where the bilinear control presents great advantages compared with PI control.

Table 2. Performance comparison between bilinear and PI control.

	PI	Bilinear	Comments
$i_{v_{dq}}$	Larger overshoots and oscillations	Smaller overshoots	Similar settling time for both
$i_{circ_{dq}}$	Good reference tracking (nonzero reference)	Steady state errors, but closer to zero	Similar oscillation
i_{circ_0}	Very good track of reference	Larger oscillations	Different references for each controller
W_h	Very good track of reference	Steady state errors	Bilinear with oscillating dynamics
W_v	Larger overshoots	Smaller overshoots	Both present steady state errors

4.2. Varying Total Converter Energy

Figure 4 aims to demonstrate the controllers' management over the converter energy. In the second graphic, $i_{v,d}$ is shown, followed by $i_{v,q}$, $i_{cir,0}$, W_h, and W_v.

For this test, the converter operating point was set to 70% of the nominal power, at 0.05 s. The converter energy reference was changed by $\pm 10\%$ from the nominal value (3.6 MJ) in this test. The seventh graphic shows the total converter energy (W_h), where either bilinear or PI controllers drive the energy to its reference value. The tracking process takes less than 50 ms for both controllers. The speed of convergence can be modified by modifying the controller gains according to the grid requirements, respecting the converter capability curve. The tracking process of total energy (W_h) implies an overshoot in state variable $i_{cir,0}$ (sixth graphic), because this state variable handles the DC output power, which is directly linked with stored energy. The PI behavior can also be regulated by gain tuning.

4.3. Disturbance in Energy Balance

One of the goals of the proposed control strategy is to keep the energy balance between the upper and lower arms of the MMC (W_v). On the previous tests (four-quadrant operation), W_v was kept around its reference value ($\bar{W}_v = 0$). Although the MMC control strategies in general aim at keeping $W_v = 0$, it would be interesting to know how the operation with $W_v \neq 0$ would influence the proposed control strategy and the behavior of the considered states. With this purpose, a disturbance is considered as an imbalance between upper and lower converter arms. A positive value of W_v means that there is more energy in the upper arms than in the lower, and a negative value means more energy in the lower arms. The eighth graphic in Figure 4 shows W_v. Each state reacts in a distinct way, as follows:

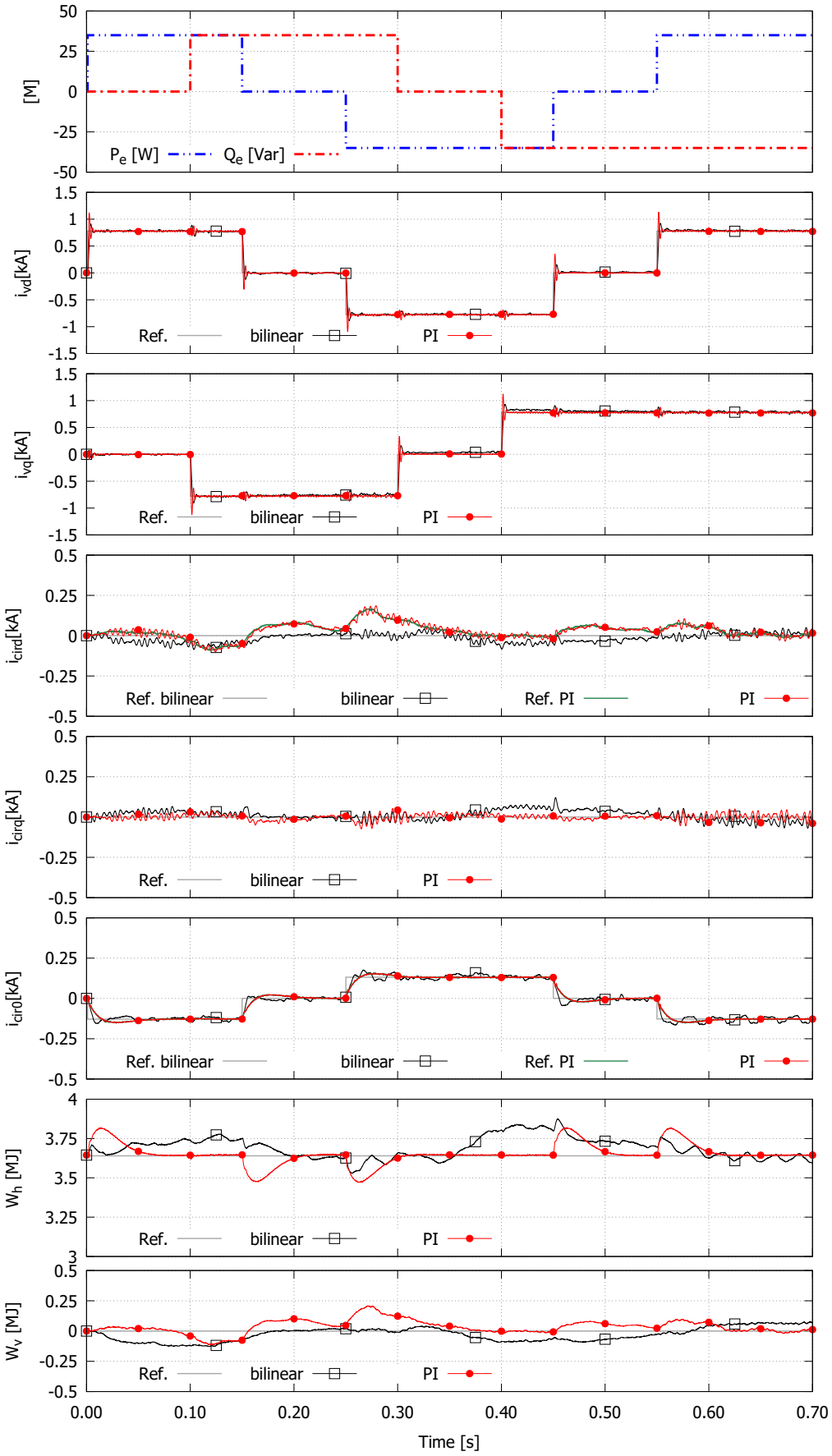

Figure 3. Bilinear and PI controllers in four-quadrant operation.

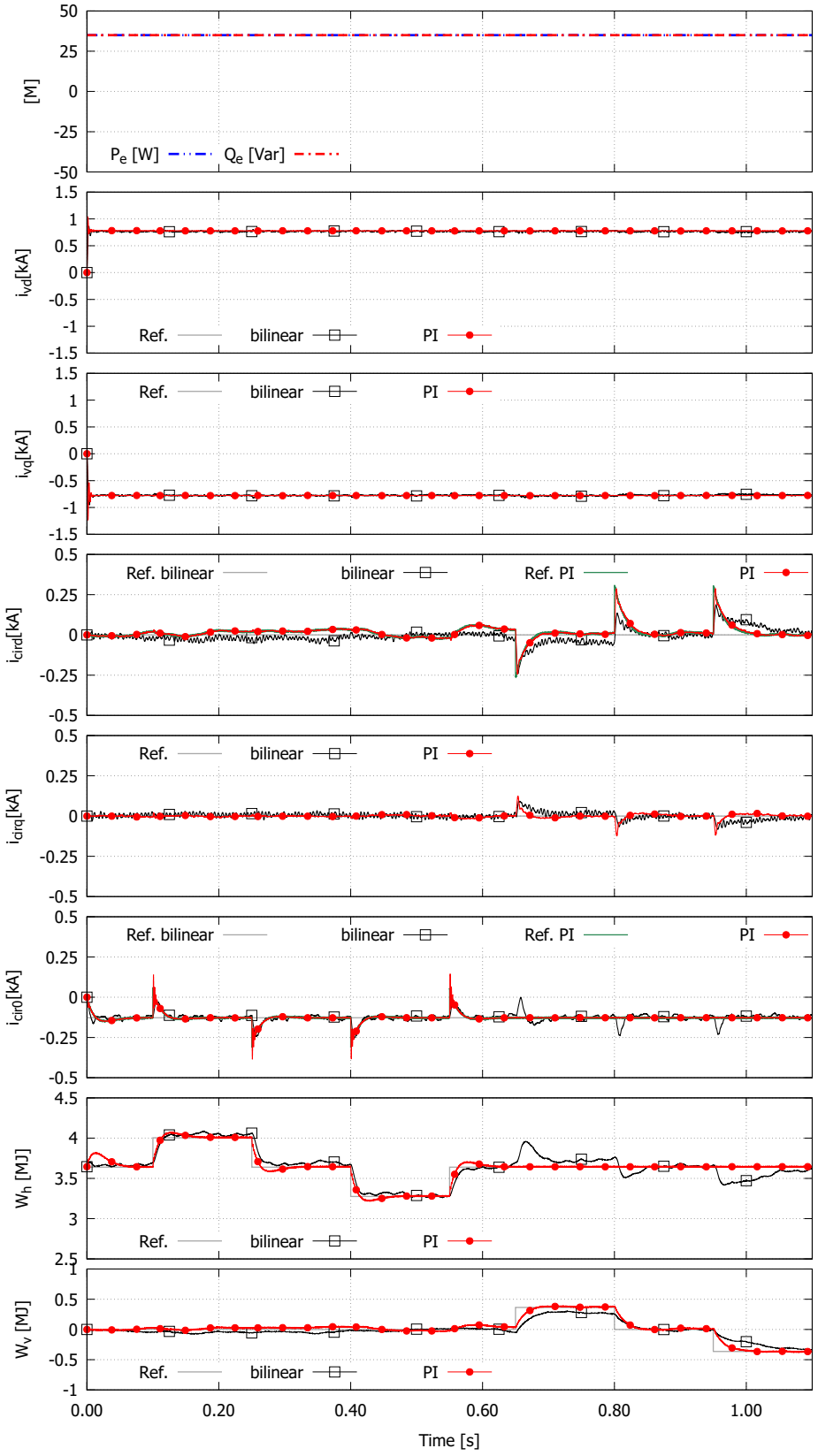

Figure 4. Bilinear and PI controllers with energy step changes.

- The fourth and fifth graphics show circulating current $i_{cir,d}$ and $i_{cir,q}$. Their behaviors are proportional to changes in W_v, more pronounced in $i_{cir,d}$ than in $i_{cir,q}$. Furthermore, to increase the upper arms' energy (at $t = 1$ s), circulating currents $i_{cir,dq}$ become

negative (which means a change in the current direction), and to balance upper and lower energies, currents become positive (at $t = 1.5$ s). They also become positive to balance lower arms at $t = 0.9$ s. PI and bilinear have similar performance.
- Under the bilinear controller, state variables $i_{cir,0}$ and W_h show overshoot for each change in W_v, while under PI, these changes do not produce overshoot.
- Lastly, the control response for an unbalanced condition of W_v is shown in the eighth graphic. It shows that bilinear control reacts at around 100 ms to drive the state to a desired reference, while PI presents a faster response.

The test presented above pointed out for bilinear control that circulating current components, $i_{cir,dq0}$, and total energy, W_h, actuate to manage the energy flow between the upper and lower converters' arms.

4.4. Robustness Analysis

A set of scenarios are created where parameter uncertainties are considered. For each scenario, one parameter (R, L, or C_{SM}) assumes $\pm$10% or $\pm$20% from its nominal value. Meanwhile, the bilinear controller is computed using the parameters' nominal values. At $t = 0.01$ s, the operating point is changed.

Figures 5 and 6 consider uncertainties in arm resistance R and inductance L. There, one may see that the bilinear control still keeps stability with a very small difference from the nominal value, even with important parameter errors. Considering the variation in resistance, the controller was able to track the references, except for state W_h. One explanation for this result is that reference calculation for i_{circ0} and W_h, Equations (31) and (35), is based on resistance value. For this reason, the controller is tracking a slightly different reference.

In the case of errors in L, one may observe a very small ($\simeq$1%) stationary error in i_{vd} and W_h; meanwhile, the other states are perfectly driven to their references in all proposed scenarios.

For C uncertainties (Figure 7), the bilinear controller tracked the references for all states well. It should be highlighted that the capacitor voltage's initial condition is the same for all the scenarios; therefore, the initial energy in each sub-module varies according to its capacitance value. That is the reason that the energy initial condition in Figure 7 is different for each value of C. However, it is interesting to note that the proposed controller steered W_h to its reference for these different initial conditions. Similar behavior is observed for the scenario when the DC voltage is different than the nominal value; see Figure 8.

Figure 9 presents state variables facing errors in AC voltage. There is a time-varying response during transitory, with a fast convergence to the desired value. The states i_{vd} and i_{vq} presented minor stationary error. This can be explained by the calculation of their references ($\bar{i}_{vd}$ and $\bar{i}_{vq}$), Equations (28) and (29), which takes into consideration the nominal values of the AC voltage.

4.5. SM Voltage Balancing

Figure 10 shows the voltage balancing of phase C lower arm sub-modules. Figure 10a shows that the voltage average value is almost constant during a 2-second simulation. Figure 10b shows in detail the voltage on each sub-module. It is noteworthy that the proposed controller regulates the total energy and energy balance between the lower and upper parts of the converter. The voltage balance among sub-modules is performed by the sorting algorithm after the PWM modulation stage. This sorting algorithm [7], however, is not a result of the present paper.

These simulations used a simulated model which is much more realistic than the one used for control design. Nevertheless, the controller was able to stabilize the system to its reference, as expected from the theoretical analysis. This illustrates the robustness of the proposed scheme.

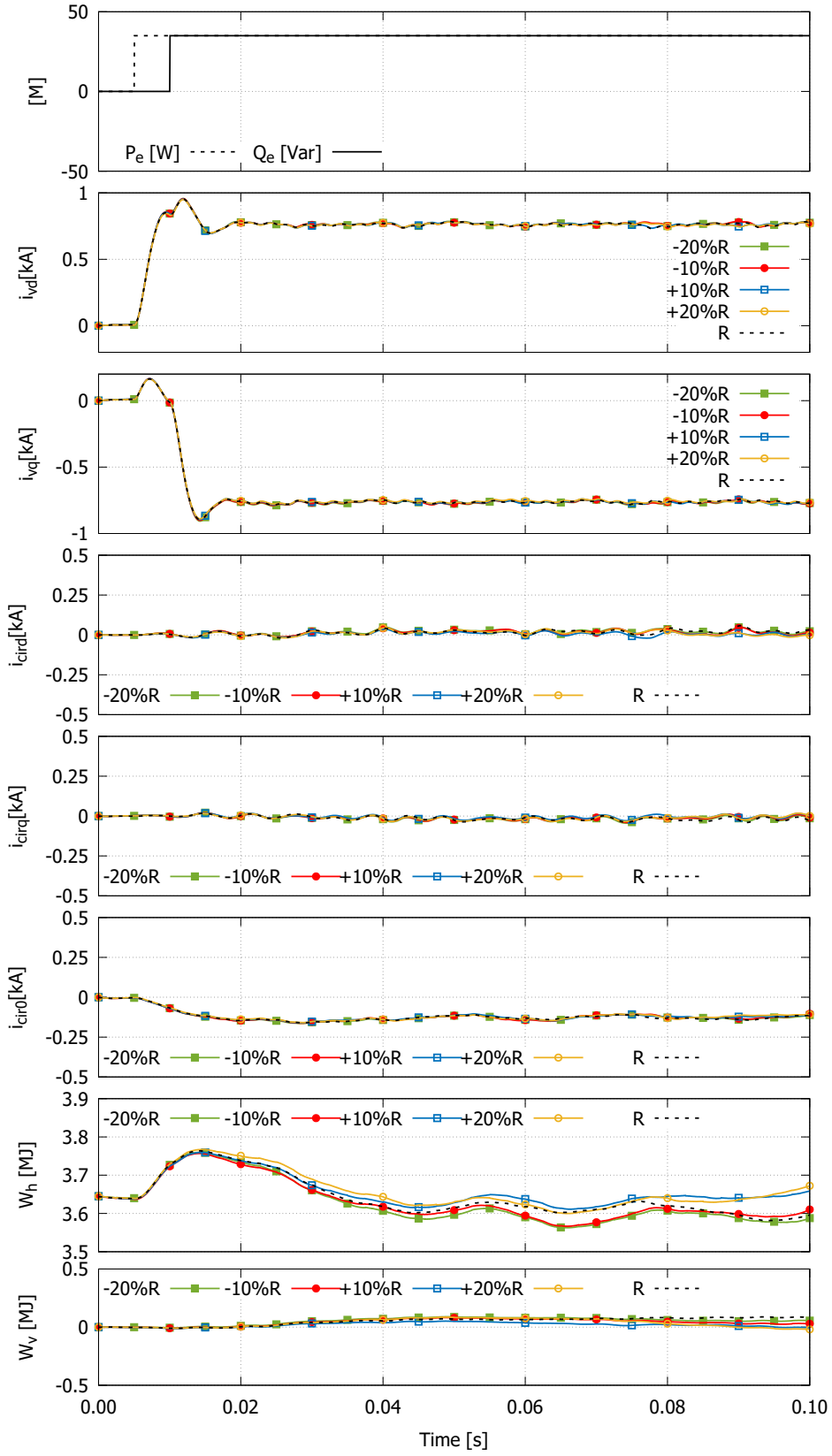

Figure 5. The system state over variation of parameter R with bilinear controller.

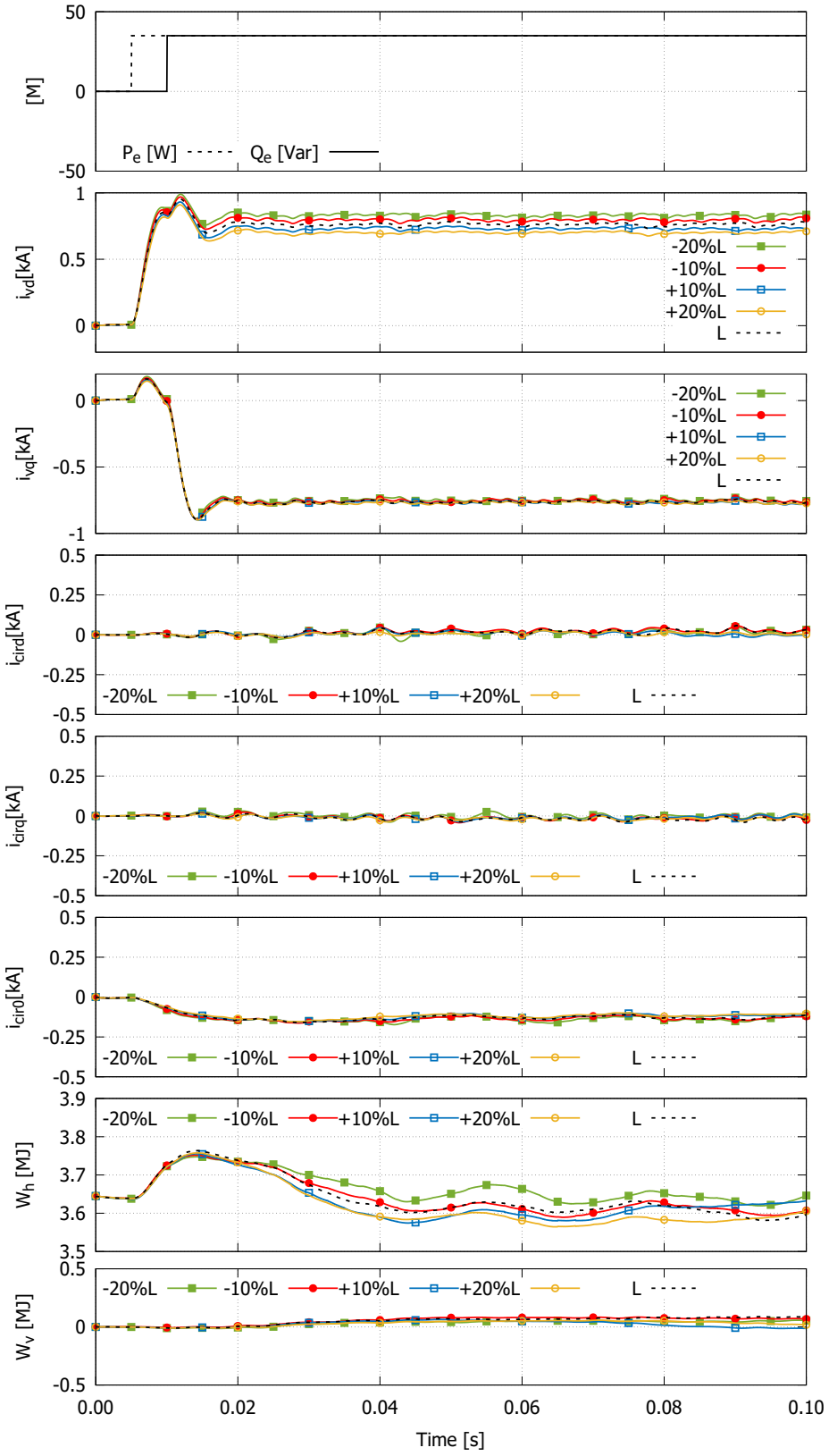

Figure 6. States over variation of parameter L with bilinear controller.

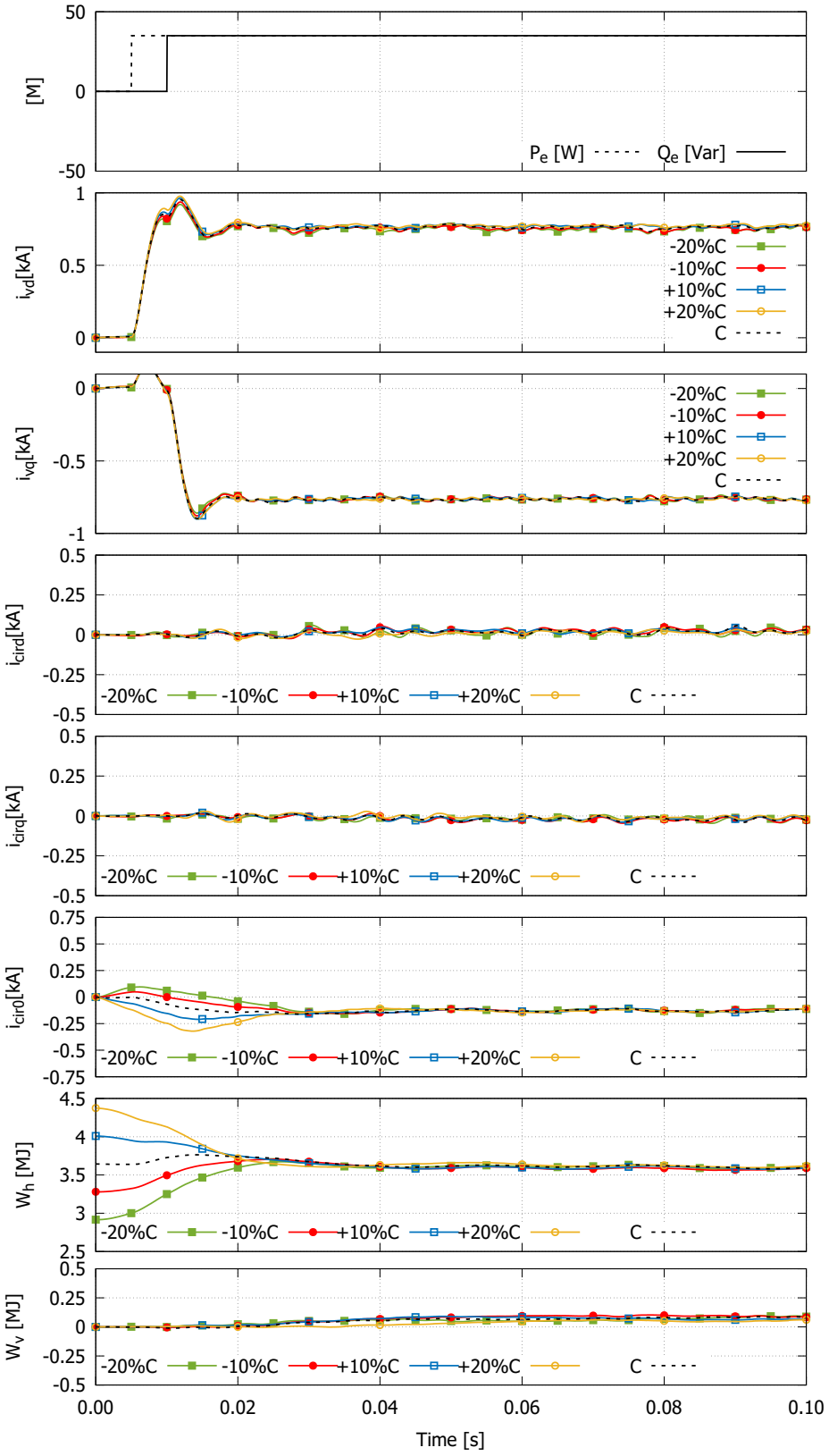

Figure 7. States over variation of parameter C with bilinear controller.

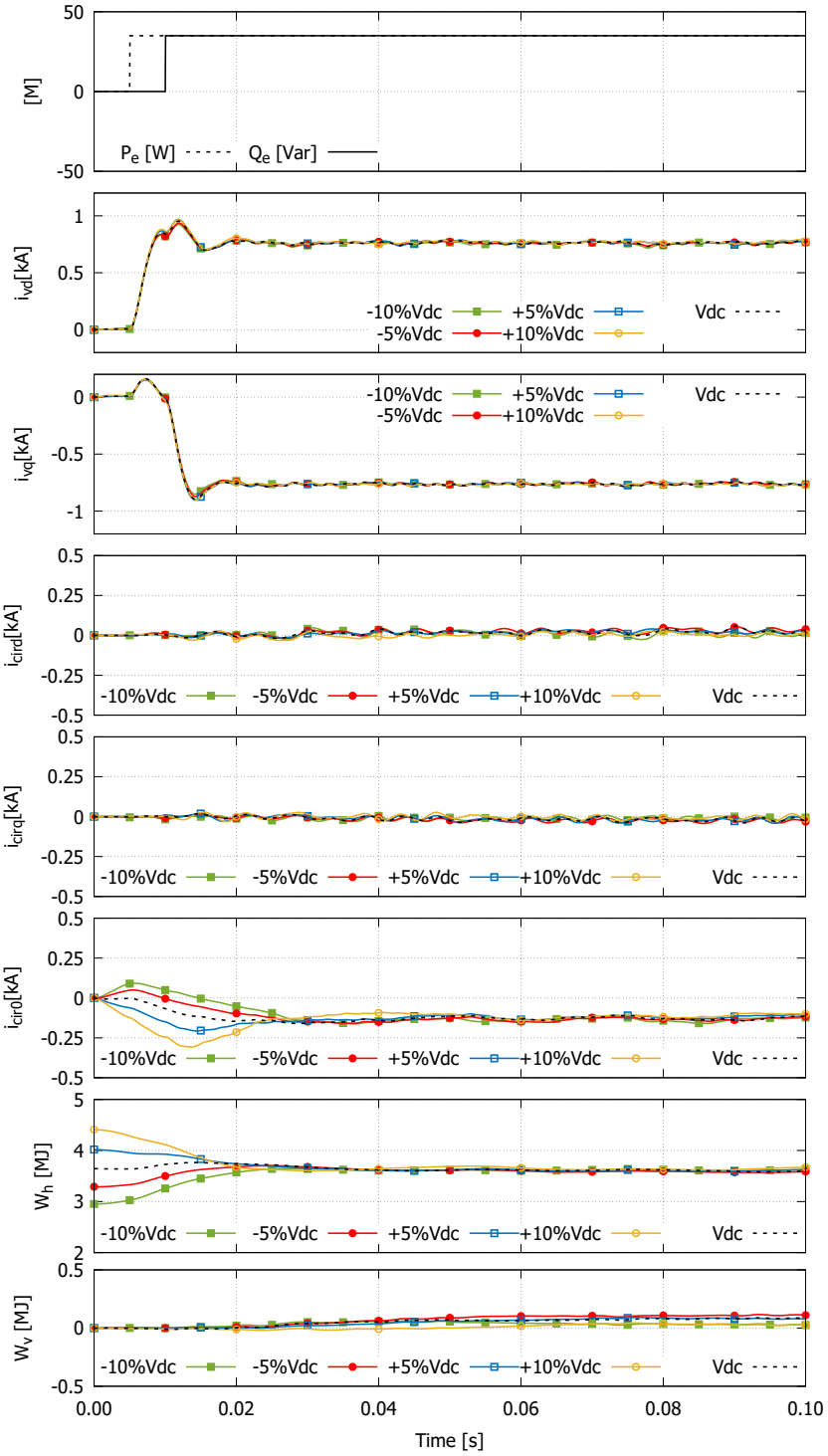

Figure 8. Fluctuation of DC voltage with bilinear controller.

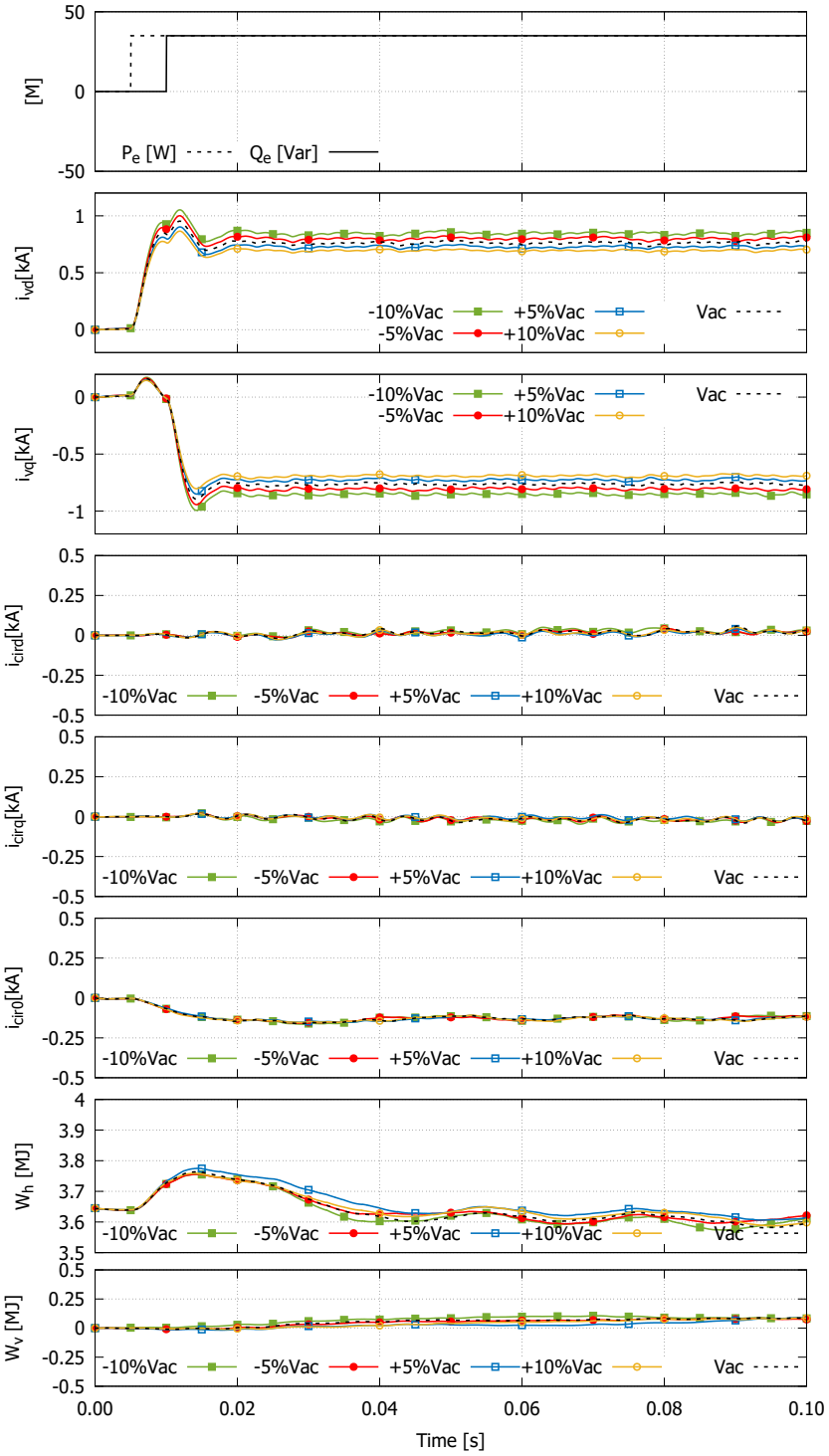

Figure 9. Error on AC voltage with bilinear controller.

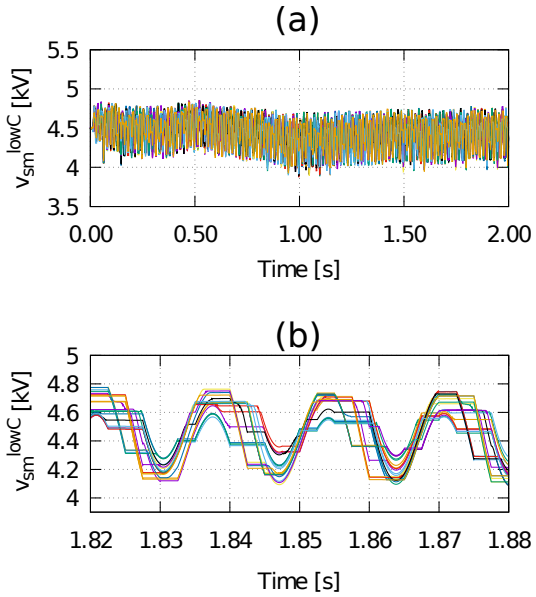

Figure 10. SMs' voltage balancing for lower arm of phase C.

5. Conclusions

This paper presents a bilinear control for an MMC converter, which directly controls all its state variables, AC, DC, and circulating currents and MMC energy, using a single control law. A rigorous mathematical proof is given for its stability, which is based on Lyapunov's theory. The controller provides asymptotic stabilization for the three-phase MMC, and the use of a Lyapunov function implies formal verification of stability and an explicit region of attraction for the considered model. Moreover, a sensitivity analysis is shown, presenting very good robustness properties for realistic parameter errors. In addition, the small number of tuning parameters, and the existence of the Lyapunov function as a guideline, make its tuning much easier than for a set of cascaded PIs, which is the standard in industry.

A bilinear control technique is simulated using a detailed switching model in the Matlab Simscape Electrical environment. The theoretical and simulated results show that the proposed controller suits MMC time response and overshoot requirements, and provides an effective trade-off between power and energy control in the converter. Moreover, the energy management provided by the bilinear controller opens the way for new ancillary services for grid support, both for AC and DC grids, such as fast frequency response or synthetic inertia.

Comparing the bilinear control with respect to standard PI control, there is a rigorous stability proof for the first, with a well-established operating range, which is not true for PI. In the simulations, the controllers showed similar performance and robustness, with an improvement in the case of the bilinear control. Future work will use experimental setups to better investigate the properties of this control system. Likewise, optimization of the control gains will be investigated to further improve the performance of the controller.

Author Contributions: Conceptualization, all authors; methodology, G.C.d.O., G.D. and R.M.M.; validation, G.C.d.O. and F.P.; formal analysis, G.C.d.O. and G.D.; investigation, all authors; writing—original draft preparation, G.C.d.O.; writing—review and editing, G.D., M.J.C., F.P. and R.M.M.; supervision, G.D. and R.M.M. All authors have read and agreed to the published version of the manuscript.

Funding: This research was supported by the Erasmus Mundus SMART2 grant number 552042-EM-1-2014-1-FR-ERA MUNDUS-EMA2 coordinated by CentraleSupelec and by CAPES Foundation-Coordenação de Aperfeiçoamento de Pessoal de Nível Superior-Brasil.

Conflicts of Interest: The authors declare no conflict of interest. The funders had no role in the design of the study; in the collection, analyses, or interpretation of data; in the writing of the manuscript, or in the decision to publish the results.

References

1. Farsi, M.; Liu, J. Nonlinear Optimal Feedback Control and Stability Analysis of Solar Photovoltaic Systems. *IEEE Trans. Control Syst. Technol.* **2020**, *28*, 2104–2119. [CrossRef]
2. Schmuck, C.; Woittennek, F.; Gensior, A.; Rudolph, J. Feed-Forward Control of an HVDC Power Transmission Network. *IEEE Trans. Control Syst. Technol.* **2014**, *22*, 597–606. [CrossRef]
3. Arrillaga, J.; Liu, Y.; Watson, N. *Flexible Power Transmission: The HVDC Options*; Wiley: Hoboken, NJ, USA, 2007.
4. Lesnicar, A.; Marquardt, R. An innovative modular multilevel converter topology suitable for a wide power range. In Proceedings of the 2003 IEEE Bologna Power Tech Conference Proceedings, Bologna, Italy, 23–26 June 2003; Volume 3, p. 6. [CrossRef]
5. Jankovic, M.; Costabeber, A.; Watson, A.; Clare, J.C. Arm-Balancing Control and Experimental Validation of a Grid-Connected MMC With Pulsed DC Load. *IEEE Trans. Ind. Electron.* **2017**, *64*, 9180–9190. [CrossRef]
6. Quester, M.; Loku, F.; El Azzati, O.; Noris, L.; Yang, Y.; Moser, A. Investigating the Converter-Driven Stability of an Offshore HVDC System. *Energies* **2021**, *14*, 2341. [CrossRef]
7. Jovcic, D.; Ahmed, K. *High Voltage Direct Current Transmission: Converters, Systems and DC Grids*; Wiley: Hoboken, NJ, USA, 2015.
8. Harnefors, L.; Antonopoulos, A.; Norrga, S.; Angquist, L.; Nee, H.P. Dynamic Analysis of Modular Multilevel Converters. *IEEE Trans. Ind. Electron.* **2013**, *60*, 2526–2537. [CrossRef]
9. Zhang, H.; Belhaouane, M.M.; Colas, F.; Kadri, R.; Gruson, F.; Guillaud, X. On comprehensive description and analysis of MMC control design: Simulation and experimental study. *IEEE Trans. Power Deliv.* **2020**, *36*, 244–253. [CrossRef]
10. de Oliveira, G.C.; Damm, G.; Monaro, R.M.; Lourenço, L.F.; Carrizosa, M.J.; Lamnabhi-Lagarrigue, F. Nonlinear control for modular multilevel converters with enhanced stability region and arbitrary closed loop dynamics. *Int. J. Electr. Power Energy Syst.* **2021**, *126*, 106590. [CrossRef]
11. Carrizosa, M.J.J.; Bergna, G.; Arzande, A.; Damm, G.; Alou, P.; Benchaib, A.; Lamnabhi-Lagarrigue, F. Stability of DC/DC three terminals converter using Modular Multilevel Converters for HVDC systems. In Proceedings of the 17th European Conference on Power Electronics and Applications (EPE-ECCE Europe 2015), Genève, Switzerland, 8–10 September 2015. [CrossRef]
12. Bergna-Diaz, G.; Freytes, J.; Guillaud, X.; D'Arco, S.; Suul, J.A. Generalized Voltage-Based State-Space Modeling of Modular Multilevel Converters With Constant Equilibrium in Steady State. *IEEE J. Emerg. Sel. Top. Power Electron.* **2018**, *6*, 707–725. [CrossRef]
13. Bergna-Diaz, G.; Suul, J.A.; Berne, E.; Vannier, J.C.; Molinas, M. Optimal Shaping of the MMC Circulating Currents for Preventing AC-Side Power Oscillations From Propagating Into HVdc Grids. *IEEE J. Emerg. Sel. Top. Power Electron.* **2019**, *7*, 1015–1030. [CrossRef]
14. Zhang, Z.; Jin, Y.; Xu, Z. Modeling and Control of Modular Multilevel Matrix Converter for Low-Frequency AC Transmission. *Energies* **2023**, *16*, 3474. [CrossRef]
15. Bergna, G.; Vannier, J.; Lefranc, P.; Arzande, A.; Berne, E.; Egrot, P.; Molinas, M. Modular multilevel converter leg-energy controller in rotating reference frame for voltage oscillations reduction. In Proceedings of the 2012 3rd IEEE International Symposium on Power Electronics for Distributed Generation Systems (PEDG), IEEE, Aalborg, Denmark, 25–28 June 2012; pp. 698–703.
16. Saad, H.; Guillaud, X.; Mahseredjian, J.; Dennetiere, S.; Nguefeu, S. MMC capacitor voltage decoupling and balancing controls. *IEEE Trans. Power Deliv.* **2014**, *30*, 704–712. [CrossRef]
17. Münch, P.; Görges, D.; Izák, M.; Liu, S. Integrated current control, energy control and energy balancing of Modular Multilevel Converters. In Proceedings of the IECON 2010—36th Annual Conference on IEEE Industrial Electronics Society, Glendale, AZ, USA, 7–10 November 2010; pp. 150–155. [CrossRef]
18. Vatani, M.; Hovd, M.; Saeedifard, M. Control of the Modular Multilevel Converter Based on a Discrete-Time Bilinear Model Using the Sum of Squares Decomposition Method. *IEEE Trans. Power Deliv.* **2015**, *30*, 2179–2188. [CrossRef]
19. Shinoda, K.; Benchaib, A.; Dai, J.; Guillaud, X. Energy control of modular multilevel converter with a novel analytic filter. In Proceedings of the 2016 18th European Conference on Power Electronics and Applications (EPE'16 ECCE Europe), Karlsruhe, Germany, 5–9 September 2016; pp. 1–10. [CrossRef]
20. Ma, Y.; Fan, L. Circulating current and DC current ripple control in MMC under unbalanced grid voltage. In Proceedings of the 2015 North American Power Symposium (NAPS), Charlotte, NC, USA, 4–6 October 2015; pp. 1–6. [CrossRef]
21. Saad, H.; Dennetière, S.; Mahseredjian, J.; Delarue, P.; Guillaud, X.; Peralta, J.; Nguefeu, S. Modular Multilevel Converter Models for Electromagnetic Transients. *IEEE Trans. Power Deliv.* **2014**, *29*, 1481–1489. [CrossRef]
22. Antonopoulos, A.; Angquist, L.; Nee, H. On dynamics and voltage control of the Modular Multilevel Converter. In Proceedings of the 2009 13th European Conference on Power Electronics and Applications, Barcelona, Spain, 8–10 September 2009; pp. 1–10.
23. Iovine, A.; Siad, S.B.; Damm, G.; De Santis, E.; Di Benedetto, M.D. Nonlinear Control of a DC MicroGrid for the Integration of Photovoltaic Panels. *IEEE Trans. Autom. Sci. Eng.* **2017**, *14*, 524–535. [CrossRef]
24. Bacha, S.; Munteanu, I.; Bratcu, A. *Power Electronic Converters Modeling and Control: With Case Studies*; Advanced Textbooks in Control and Signal Processing; Springer: London, UK, 2013.
25. Mohler, R.R. *Bilinear Control Processes: With Applications to Engineering, Ecology, and Medicine*; Mathematics in Science and Engineering; Elsevier Science: Amsterdam, The Netherlands, 1974.
26. Pardalos, P.M.; Yatsenko, V. *Optimization and Control of Bilinear Systems*; Springer: Berlin/Heidelberg, Germany, 2009.
27. Carrizosa, M.J.; Damm, G.; Benchaib, A.; Alou, P.; Netto, M.; Lamnabhi-Lagarrigue, F. Bilinear and nonlinear control algorithms for a DC/DC converter for Multi-Terminal HVDC networks. *IFAC Proc. Vol.* **2014**, *47*, 523 – 528. [CrossRef]

28. Pardalos, P.; Yatsenko, V. *Optimization and Control of Bilinear Systems: Theory, Algorithms, and Applications*; Springer Optimization and Its Applications; Springer: Berlin/Heidelberg, Germany, 2008.
29. Landau, I. *On the Optimal Regulator Problem and Stabilization of Bilinear Systems*; Laboratoire d'Automatique (CNRS): Grenoble, France, 1979.
30. Panteley, E.; Loría, A. Synchronization and Dynamic Consensus of Heterogeneous Networked Systems. *IEEE Trans. Autom. Control* **2017**, *62*, 3758–3773. [CrossRef]
31. Yazdani, A.; Iravani, R. *Voltage-Sourced Converters in Power Systems*; Wiley Online Library: Hoboken, NJ, USA, 2010; Volume 34.